LAWRENCE
LIVERMORE
NATIONAL
LABORATORY

UCRL-CONF-227160

Richtmyer-Meshkov instability-induced mixing: initial conditions modeling, three-dimensional simulations and comparisons to experiment

M. Latini, O. Schilling, W. S. Don

January 10, 2007

International Workshop on the Physics of Compressible Turbulent Mixing
Paris, France
July 17, 2006 through July 21, 2006

e-mail: schilling1@llnl.gov

Richtmyer-Meshkov instability-induced mixing: initial conditions modeling, three-dimensional simulations and comparisons to experiment

Marco LATINI[1], Oleg SCHILLING[2] and Wai Sun DON[3]

[1] *California Institute of Technology, Pasadena, California 91125, USA*
[2] *University of California, Lawrence Livermore National Laboratory, Livermore, California 94551, USA*
[3] *Brown University, Providence, Rhode Island 02912 USA*

Abstract: Turbulent transport and mixing in the reshocked multi-mode Richtmyer-Meshkov instability is investigated using three-dimensional ninth-order weighted essentially non-oscillatory simulations. A two-mode initial perturbation with superposed random noise is used to model the Mach 1.5 air/SF_6 Vetter-Sturtevant [1] experiment. The mass fraction isosurfaces and density cross-sections show the detailed structure before, during, and after reshock. The effects of reshock are quantified using the baroclinic enstrophy production, buoyancy production, and shear production terms. The mixing layer growth agrees well with the experimental growth rate. The post-reshock growth is in good agreement with the Mikaelian reshock model [2].

1 INTRODUCTION

The purpose of this research is to study turbulent transport in multi-mode Richtmyer-Meshkov instability with reshock using three-dimensional ninth-order weighted essentially non-oscillatory (WENO) simulations for the development/validation of turbulent mixing and subgrid-scale models, using the following methodology: (1) the high-resolution, finite-difference based, Eulerian, shock-capturing WENO method is applied to a model of the Vetter-Sturtevant Richtmyer-Meshkov instability shock tube experiment with reshock; (2) validation is performed by comparing to experimental amplitude data, and simulations/analysis are extended to longer times than in experiment; (3) Favre-averaged quantities used in turbulence models are computed from the simulation data; (4) budgets of terms in turbulent transport equations are investigated to determine which physical processes are most important to model; (5) quantities needed in gradient-diffusion (eddy viscosity) closure models are computed.

2 EQUATIONS SOLVED AND THE METHOD

Simulations were performed using the finite-difference characteristics-based weighted essentially non-oscillatory method. The Euler equations were augmented by the mass fraction to track the mixing dynamics:

$$\frac{\partial}{\partial t}\begin{bmatrix}\rho\\ \rho u\\ \rho v\\ \rho w\\ E\\ \rho m\end{bmatrix}+\frac{\partial}{\partial x}\begin{bmatrix}\rho u\\ \rho u^2+p\\ \rho u v\\ \rho u w\\ (E+p)u\\ \rho m u\end{bmatrix}+\frac{\partial}{\partial y}\begin{bmatrix}\rho v\\ \rho u v\\ \rho v^2+p\\ \rho v w\\ (E+p)v\\ \rho m v\end{bmatrix}+\frac{\partial}{\partial z}\begin{bmatrix}\rho w\\ \rho u w\\ \rho v w\\ \rho w^2+p\\ (E+p)w\\ \rho m w\end{bmatrix}=0\,. \tag{2.1}$$

The system was solved using Lax-Friedrichs flux-split finite-difference reconstruction. A convex nonlinearly-weighted combination of all polynomial flux reconstructions is used to achieve the *essentially non-oscillatory* property and ninth-order reconstruction in smooth regions. The boundary conditions were symmetry in the transverse shock direction and reflecting at the shock tube end wall. Although the simulations presented here are Euler, the numerical viscosity acts as a surrogate for real dissipation in implicit large-eddy simulations. The ninth-order reconstruction was used for its desirable properties of reducing the numerical dissipation and preserving small-scale structures [5].

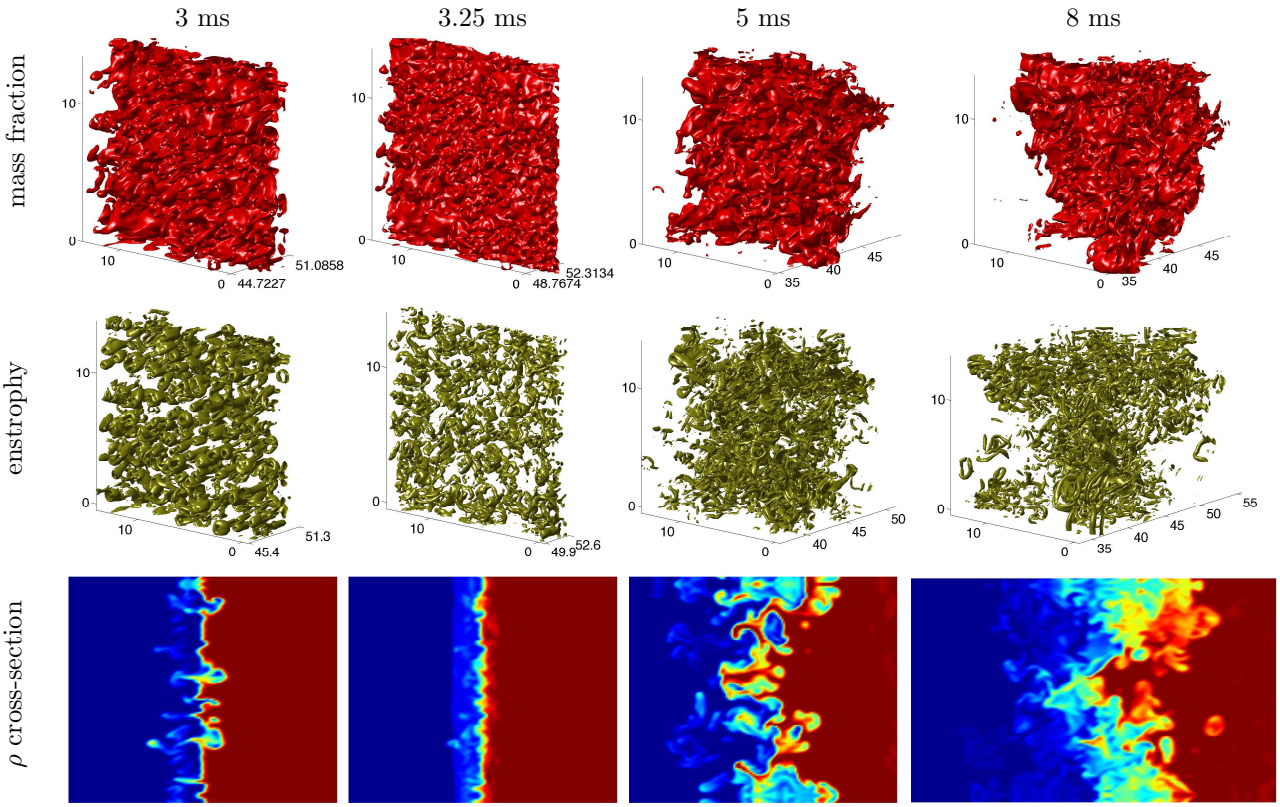

Fig. 4.1. Visualization of the mass fraction isosurface (top row), enstrophy isosurface (middle row) and density (x, y)-cross-section (bottom row) at 3, 3.25, 5, and 8 ms.

3 THE MODEL OF THE INITIAL CONDITIONS

A two-mode initial perturbation with random noise was used to model the $Ma = 1.5$ air/SF_6 Vetter-Sturtevant [1] shock tube experiment with a membrane pushing on a wire mesh. The initial conditions adopt a two-mode model of Cohen et al. [3], but with random noise similar to the work of Hill et al. [4],

$$\eta(y,z) = a\left|\sin\left(\frac{10\pi y}{27}\right)\right|\left|\sin\left(\frac{10\pi z}{27}\right)\right| - b\cos\left(\frac{2\pi y}{27}\right)\cos\left(\frac{2\pi z}{27}\right) + \psi(y,z)\,. \tag{3.1}$$

The first term models a membrane pushed through the wire mesh, the second term the mesh distortion, and the noise $\psi(y, z)$ the membrane fragmentation. The noise is super-imposed to break symmetry and accelerate the development of nonlinearity. However, as shown below, reshock is necessary to achieve a sufficiently complex mixing layer so that applying turbulent averages is meaningful [6, 7]. Simulations were performed on a domain $[0, L_x] \times [0, L_y] \times [0, L_z]$, where $L_x = 61$ and $L_x = L_y = 27$ cm (matching the test section of the Vetter-Sturtevant experiment), on a $513 \times 257 \times 257$ grid, using a pre-shock Atwood number $A^- = 0.641$ and initial parameters $a = 0.0675$ and $b = 0.00675$ cm (0.25% and 0.025% of L_z, respectively).

4 INSTABILITY DYNAMICS AND THE EFFECTS OF RESHOCK

The instability dynamics and vorticity are visualized using the mass fraction isosurface and enstrophy isosurface on the air (spike) side in Fig. 4.1. Reshock occurs at 3.25 ms and the reflected rarefaction wave arrives at 5 ms. Following reshock, the instability develops complex structure while the enstrophy transforms from elongated tubular structures into disordered short tubular structures with random orientations. The density cross-sections also aid in illustrating the development of a well-mixed complex layer.

The effects of reshock are investigated by considering key terms in the enstrophy and turbulent kinetic

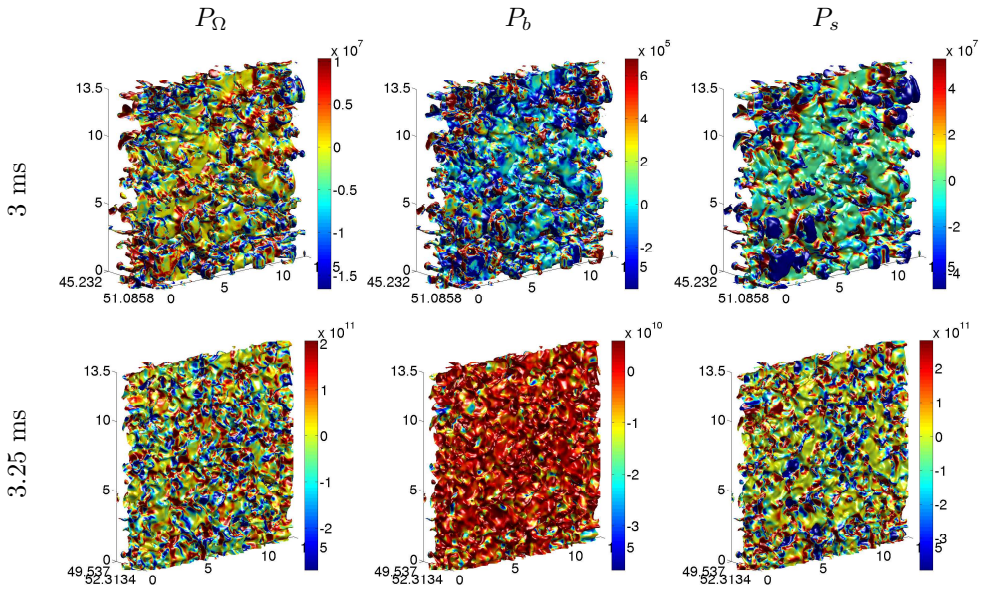

Fig. 4.2. The baroclinic enstrophy production P_Ω, buoyancy production P_b, and shear production P_s immediately before and after reshock (3 and 3.25 ms, respectively).

energy equations

$$\rho \frac{\mathrm{d}\Omega}{\mathrm{d}t} = P_\Omega + S_\Omega + C_\Omega\,, \quad P_\Omega \equiv \frac{\boldsymbol{\omega}}{\rho}\cdot(\boldsymbol{\nabla}\rho\times\boldsymbol{\nabla}p) \quad S_\Omega \equiv \rho\boldsymbol{\omega}\cdot(\boldsymbol{\omega}\cdot\boldsymbol{\nabla}\boldsymbol{u}) \quad C_\Omega \equiv -2\,\rho\,\Omega\,\boldsymbol{\nabla}\cdot\boldsymbol{u}\,, \tag{4.1}$$

$$\overline{\rho}\frac{\mathrm{d}\widetilde{E''}}{\mathrm{d}t} = P_b + P_s + T + D + \Pi\,, \quad P_b \equiv \overline{u_j''}\frac{\partial\overline{p}}{\partial x_j} \quad P_s \equiv \overline{\rho\,u_i''u_j''} \quad T \equiv -\frac{\partial}{\partial x_j}\left(\overline{\rho E''u_j''} + \overline{p'u_j''} - \overline{u_i''\sigma_{ij}''}\right) \tag{4.2}$$

$$D \equiv -\overline{\sigma_{ij}''\frac{\partial u_i''}{\partial x_j}} \quad \Pi \equiv \overline{p'\frac{\partial u_i''}{\partial x_i}}\,,$$

where $\overline{\phi}(z,t) = \frac{1}{L_x\,L_y}\int_0^{L_y}\int_0^{L_x}\phi(\mathbf{x},t)\mathrm{d}x\mathrm{d}y$ and $\phi(\mathbf{x},t)' = \phi(\mathbf{x},t) - \overline{\phi}(z,t)$, are the Reynolds average and fluctuating fields, respectively and $\widetilde{\phi}(z,t) = \overline{\rho\,\phi}/\overline{\rho}$ and $\phi(\mathbf{x},t)'' = \phi(\mathbf{x},t) - \widetilde{\phi}(z,t)$ are the Favre average and fluctuating fields, respectively.

Figure 4.2 shows the baroclinic enstrophy production, P_ω, buoyancy production, P_b, and shear production P_s at 3 and 3.25 ms, illustrating the amplification caused by reshock.

5 COMPARISON OF THE MIXING LAYER WIDTH WITH EXPERIMENTAL DATA AND THE MIKAELIAN RESHOCK MODEL

From the mass fraction fields define the bubble and spike position $\ell_s(t)$ and $\ell_b(t)$ as the locations where $m < 0.01$ and $m > 0.99$, respectively. The mixing layer width, $h(t) = \ell_b(t) - \ell_s(t)$, is shown in Fig. 5.3. The growth rates agree with the Vetter and Sturtevant experimental measurements 0.4 cm/ms (before reshock) and 3.26 cm/ms (after reshock). The WENO mixing layer width also agrees with the experimental data after reshock and overpredicts beforre reshock. It is hoped that smaller values of a (requiring increased resolution) may provide better agreement with the pre-reshock data. The post-reshock mixing layer width was also compared to Mikaelian's prediction [2]

$$h(t) = 0.28\,A_1^+\,\Delta u_1\,t\,, \tag{5.1}$$

where A_1^+ is the post-reshock Atwood number and Δu_1 is the change in velocity interface after reshock.

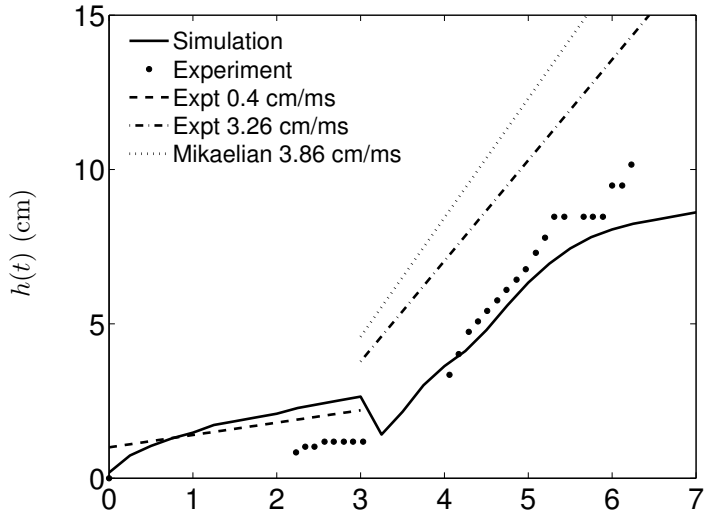

Fig. 5.3. Comparison of the mixing layer width from the simulation with the Vetter-Sturtevant [1] experimental growth rates and data points and the prediction of the Mikaelian [2] reshock model.

6 SUMMARY AND CONCLUSIONS

Constructed in this work was a two-mode initial perturbation with random noise to model the complex mixing layer in the reshocked $Ma = 1.5$ air/SF_6 Vetter-Sturtevant [1] experiment. The random noise is needed to break symmetry and accelerate the development of nonlinearity. A visualization of the instability through the mass fraction isosurface and enstrophy isosurface was presented. The effects of reshock were quantified by measuring the baroclinic enstrophy production, buoyancy production, and shear production terms on the mass fraction isosurface. In all cases Reshock amplifies these quantities. The enstrophy isosurface also shows a qualitative change after reshock from long elongated tubes aligned along the direction of shock propagation to small short tubular structures with random orientations. This indicates that reshock is essential to achieve a sufficiently complex layer where turbulent averages become meaningful. The mixing layer widths for simulations with different values of the initial conditions parameters were compared. The pre-shock amplitude was sensitive to the large-scale parameter a, while the post-reshock amplitude was sensitive to the relative ratios of the large- and small-scale parameters a/b. The growth of the mixing layer agreed with the experimental measured growth and the prediction of the Mikaelian [2] reshock model. The WENO amplitude over-predicted the experimental amplitudes before reshock but were in agreement after reshock.

The results from this investigation indicate that high-resolution simulations can be used to provide essential data concerning turbulent transport and mixing processes in three-dimensional reshocked Richtmyer-Meshkov instability.

REFERENCES

[1] Vetter, M. and Sturtevant, B. 1995. Experiments on the Richtmyer-Meshkov instability of an air/SF_6 interface. *Shock Waves* **4**, pp. 247–252.

[2] Mikaelian, K. O., 1989. Turbulent mixing generated by Rayleigh-Taylor and Richtmyer-Meshkov instabilities. *Physica D* **36**, pp. 343–357.

[3] Cohen, R. H., Dannevik, W. P., Dimits, A. M., Eliason, D. E., Mirin, A. A., Zhou, Y., Porter, D. H. and Woodward, P. R. 2002. Three-dimensional simulation of a Richtmyer-Meshkov instability with a two-scale initial perturbation. *Phys. Fluids* **14**, pp. 3692–3709.

[4] Hill, D. J. and Pullin, D. I., 2004. Hybrid tuned center-difference-WENO method for large eddy simulations in the presence of strong shocks. *J. Comput. Phys.* **194**, pp. 435–450.

[5] Latini, M., Schilling, O. and Don, W. S. 2007. Effects of WENO flux reconstruction order and spatial resolution on reshocked two-dimensional Richtmyer-Meshkov instability. *J. Comput. Phys.*, in press.

[6] Latini, M., Schilling, O. and Don, W. S. 2007. High-resolution simulations and modeling of reshocked single-mode Richtmyer-Meshkov instability: comparison to experimental data and to amplitude growth model predictions. *Phys. Fluids*, in press.

[7] Schilling, O., Latini, M. and Don, W. S. 2007. Physics of reshock and mixing in single-mode Richtmyer-Meshkov instability. *Phys. Rev. E*, submitted.